Ibn Al-Haitham Journal for Pure and Applied Sciences
Journal homepage: jih.uobaghdad.edu.iq
PISSN: 1609-4042, EISSN: 2521-3407
IHJPAS. 2025, 38(4)

Effect of Thermal Neutron Irradiation on the Electrical Properties of Lead-Selenium Substituted $S_{70}Se_{30-X}Pb_X$ Chalcogenide Glasses

Mahmoud Y. Hajem[1*] and Kareem A. Jasim[2]
[1, 2] Department of Physics, College of Education for Pure Science (Ibn Al-Haitham), University of Baghdad. Baghdad, Iraq.
[*]Corresponding author

Received:20 January 2025 Accepted:5 May 2025 Published:20 October 2025
doi.org/10.30526/38.4.4115

Abstract.

This study included the effect of thermal neutron radiation and partial replacement of selenium with lead for $S_{70}Se_{30-x}Pb_x$ alloy samples with different lead concentrations **(**x = 0 and 5) prepared by the melting point technique. The samples were examined before and after thermal neutron irradiation for seven days with Am^{241}–Be^{9} radioactive source, with a radiation dose of $6.048 * 10^5$ n.cm^{-2} . Continuous electrical conductivity analysis revealed changes in all samples, attributed to the rearrangement of the crystal structure caused by radiation-induced disturbances. These changes led to modifications in the electrical properties of the irradiated samples compared to the non-irradiated ones. compared to the non-irradiated ones. Three different conduction mechanisms were found. At low temperatures, the electron transition occurred via electron hopping between localized states close to the Fermi energy. At intermediate temperatures, the conduction occurred via electron hopping between localized levels between the tails of the conduction and valence bands. The electrons moved through extended levels within the two bands at high temperatures. The results indicated that the calculated densities of extended, localized, and Fermi-level states underwent significant changes due to thermal neutron radiation and partial substitution.

Keywords: Melting point, Radiation dose, Thermal neutron radiation, Electrical properties, Electron hopping, Electrical conductivity.

1. Introduction

Amorphous chalcogenide semiconductors have been extensively studied and often exhibit typical P-type behavior characteristics, largely due to the abundance of localized states near the Fermi energy and within the energy gap, where the Fermi level is effectively fixed (1–3). These materials have become more technologically viable when metal additives or partial substitutions of their chemical components are added (4), which enhance their conductivity and significantly reduce the activation energy required for conduction (5).

According to the Mott–Davies model, the valence requirements of chalcogenides are usually met for all elements (6). This model explains the slight changes in electrical and optical behavior in doped chalcogenides. Studies have shown that the introduction of some chemical elements, such as bismuth, can significantly enhance the P-type conductivity, increasing by more than 7% compared to N-type materials (7). On the other hand, the addition of elements

such as indium, antimony, or tin has generally led to the formation of P-type compounds (8, 9). Since not all impurities are electrically active, the concentration of impurities is a crucial factor in determining their effect (10, 11). Therefore, understanding the effect of impurities on the properties of chalcogen glasses is essential for both fundamental and applied research (12, 13).

Experimental evidence indicates that the introduction of impurities into binary systems such as Se-Te-Sn or Ge-Te-Sb significantly changes the electrical properties of chalcogen glasses (14). In addition, the glass composition, impurity chemistry, and activation methods have a significant impact on the behavior of the material (15). For example, it was studied the effect of indium on the density of local and extended states and the Fermi level, and revealed a change in the density of local and extended states and the Fermi level when increasing the indium concentrations of $Se_{85}Te_{10}Sn_{5-x}In_x$ alloys to include changes in the activation energy, tail width, and inter-state distance, as well as an increase in the density of local and extended states and the Fermi level (14).

When the $Ge_{30}Te_{70-x}Sb_x$ alloy was partially replaced, the density of local and extended states and the Fermi level were examined, and it was found that all energy states, including the activation energy, tail width, inter-atomic distances, and transition distance, were changed (15). Researchers (10-13) focused on studying the electrical properties of $Se_6Te_{4-x}Sb_x$ and $Se_6Te_{4-x}Sn_x$ alloys by partially substituting tellurium with antimony, and the energy density of several energy states, including the electronic hopping distance, Fermi level, locality, and tail width, were calculated. They concluded that the energy state density increases with the change in the concentration of substituted elements. One of the distinctive properties of amorphous chalcogen semiconductors is their sensitivity to external influences, especially ionizing radiation with an average energy exceeding 1 MeV (16, 17). In this study, the $S_{70}Se_{30-x}Pb_x$ alloy with (x = 0 and 5) ratios will be prepared using the melting point method and the effect of partial substitution of selenium with lead on the electrical properties and the density of states within the energy gap and in the conduction and valence bands will be studied.

2. Materials and Methods

Two samples of $Se_{70}Se_{30-x}$-Pb_x alloy were prepared by partial replacement of selenium with lead in ratios X = (0, 5) using the melting point method according to the following **Equation 1**:

$$70S + (30-x)\,Se + Pb_x = Se_{70}Se_{30-x}Pb_x \quad (1)$$

The alloys were prepared from their constituent elements sulfur (S), selenium (Se) and lead (Pb) with high purity (99.999%). The constituent elements of the alloys were weighed according to the specified weight ratio. The components were then mixed, crushed, and placed in quartz 5 tubes, which were tightly sealed after being evacuated to a pressure of 10^{-3} Pa using a vacuum pump. Then, the evacuated capsules were placed in an electric furnace, and the temperature of the furnace was gradually raised at a rate of 10°C per minute until reaching a temperature of 350 °C. The samples were kept in the furnace for 3 hours at this temperature. Then, the temperature of the electric furnace was reduced at the same rate of ascent, and the capsules were left inside the furnace to cool slowly and gradually for 24 hours. Then the capsules were extracted from the electric furnace and broken to extract the molten material very carefully from each capsule separately. Then the components of each sample were crushed until the samples were ready for pressing using a hydraulic press.

They were formed into small discs with dimensions of 1.5 cm in diameter and 0.4 cm thick under a pressure of 7 tons/cm². Then the electrical resistance of each sample was calculated as the samples were placed separately and individually in the electric furnace and the electrical resistance was studied with a change in temperature from 24 to 200 degrees Celsius by connecting each disc to an electrical circuit with two poles connected to a device (digital ohmmeter) as shown in **Figure 1** and a specific voltage difference was applied between the two ends of the sample and it automatically measures the amount of current passing through the sample, and through an electronic screen in the digital ohmmeter the value of the electrical resistance appears. Then all samples were placed in a special device containing a radioactive source, which is (Am241-Be9).

For seven days, all samples were exposed to a thermal neutron flux of 6.04 × 1010 ($n.cm^{-2}$). In the same way as above, the electrical resistance of each sample was calculated, as the samples were placed separately and individually in the oven, and the electrical resistance was calculated with a change in temperature from 24 to 200 degrees Celsius.

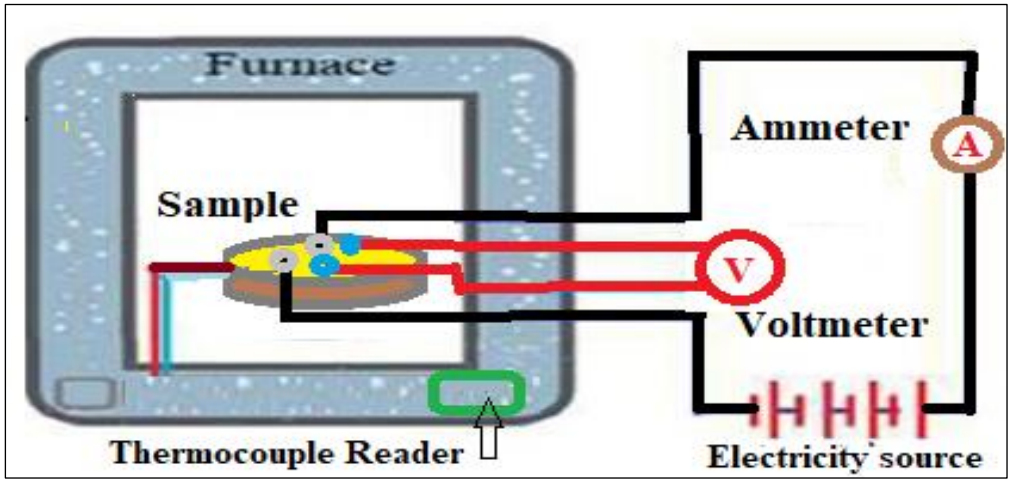

Figure 1. The electrical circuit of the digital ohmmeter

3. Results and Discussion

The specific resistivity of the S70Se30-x-Pbx alloy was measured for each X value (X = 0 and 5) within the temperature range of 297 to 473 K, using the method illustrated in **Figure 1**. In **Figure 2**, which represents the relationship between specific resistivity and temperature change, the specific resistivity at certain temperatures for all samples decreases with the change in lead addition. This occurs as a result of the partial replacement of selenium by lead in both samples, while the properties of the alloys remained those of semiconductors. Also, increasing the lead content in the alloys has a clear effect when the temperature increases. In addition, it was observed that the electrical resistivity changed with the increase in lead concentration in the electrical resistivity of S70Se30-x-Pbx alloy composite was tested for each value of X for two samples (X = 0 and 5) within the temperature range of 297 and 473 K. This is because lead is a metallic element with high conductivity like other metals, but it shows a small electrical resistance, which leads to an increase in its concentration in the alloy, which leads to a decrease in electrical resistance at a lead concentration of 5.

This change is due to a change in the electronegativity of the alloy due to the partial replacement of selenium with lead between the two elements that make up the prepared alloy, as well as the sizes of the atoms of the lead element are larger than the sizes of the atoms of the elements that make up the alloy because the diameter of the lead element atom is larger than the diameters of the other atoms that make up the alloy. This leads to expansion in the crystal lattice, internal distortions and stresses, crystal defects, and changes in the electrical

properties of the alloy, which leads to the formation of a more stable compound when the ratio x equals 5.

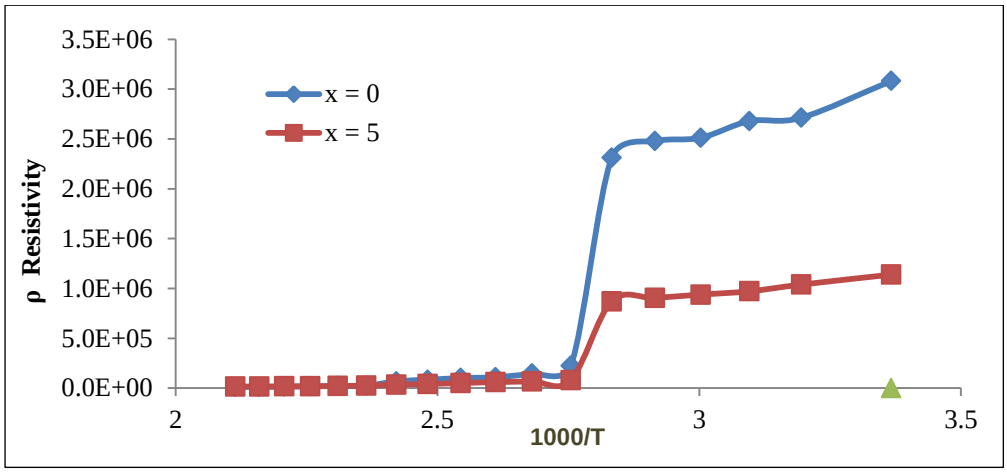

Figure 2. Shows the relationship between the electrical resistivity ρ and 1000/T for $Se_{70}Se30\text{-}xPb_x$ as a function of the concentration ratio (X = 0 and 5) before irradiation.

After irradiation, the electrical resistivity of two samples (X = 0 and X = 5) was measured at specific temperatures, as shown in **Figure 3**. The electrical resistivity of the $S_{70}Se_{30-x}Pb_x$ compound was evaluated for each prepared concentration within the temperature range of 297–473 K. It was observed that the resistivity of both samples changed after exposure to the thermal neutron dose. At X = 0, the electrical resistivity decreased due to improved regularity in the crystal structure caused by radiation exposure. In contrast, at X = 5, the resistivity increased due to distortions in the crystal structure, as thermal neutron radiation induced structural instability. This instability influenced the crystal's regularity, leading to different resistivity behaviors at varying concentrations. Additionally, a sudden increase in electrical behavior at the same temperature in both cases may indicate a transition from insulating to semiconducting behavior, where charge carriers are excited into the conduction band. Neutron irradiation can also cause defect rearrangement, enhancing electron mobility and thereby reducing resistivity. Furthermore, a phase transition at this temperature could alter the material's structure, significantly impacting its electrical conductivity.

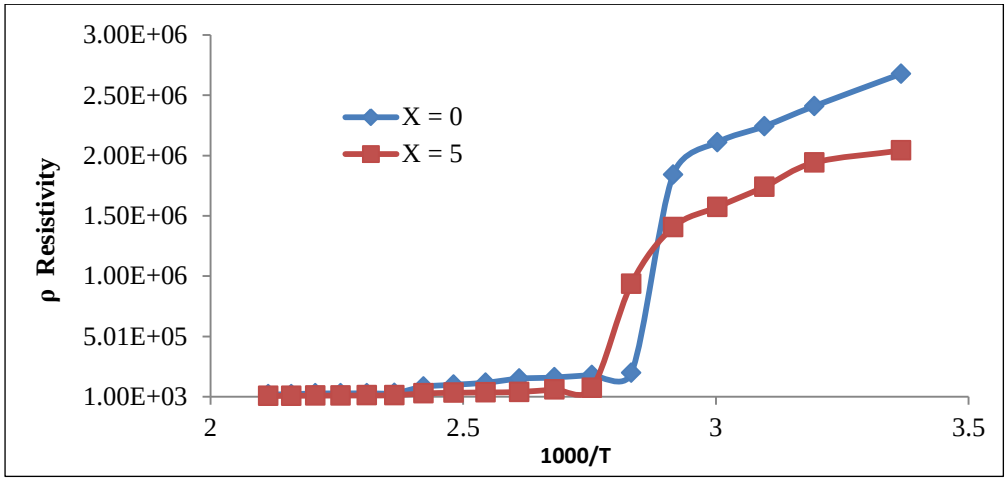

Figure 3. Shows the relationship between the electrical resistivity ρ and 1000/T for $Se_{70}Se_{30\text{-}x}\text{-}Pb_x$ as a function of the concentration ratio (X = 0 and 5) after irradiation

The electrical resistivity was calculated at temperatures in the temperature ranges between (297-473) K for the alloy samples $S_{70}Se_{30\text{-}X}Pb_X$ and according to the lead concentration (X = 0 and 5) and using the two-point test method, the electrical resistivity of the alloy samples was recorded as a function of temperature, and then the electrical resistivity was calculated as

a function of temperature as shown in the curves in **Figure 4**.

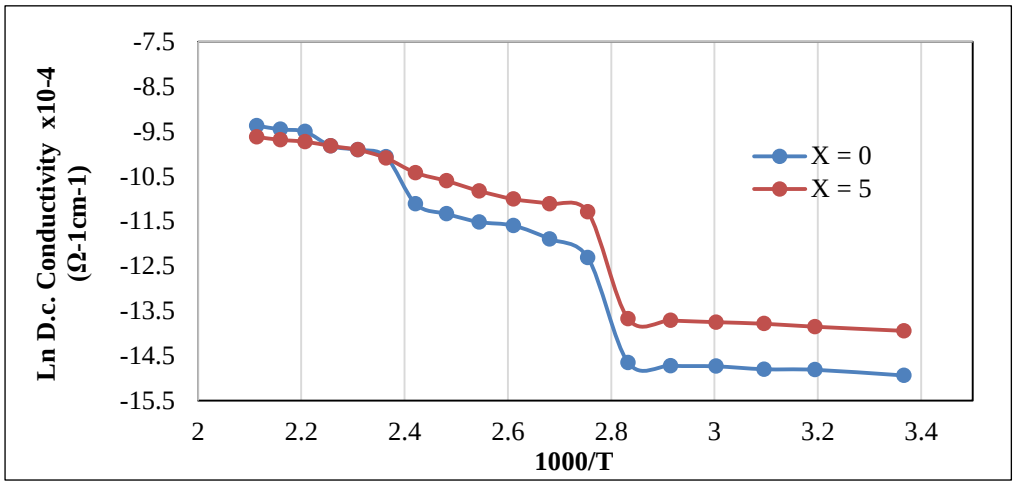

Figure 4. Electrical conductivity (DC) Ln (σ) of $S_{70}Se_{30-X}Pb_X$ as a function of 1000/T and according to the concentration ratio (X = 0 and 5) before irradiation.

The logarithmic relationship between the electrical conductivity and absolute temperature is shown in **Figure 1** before irradiation and **Figure 5** after irradiation, showing how the electrical conductivity Ln (σ) and 1000/T change. The data show that all samples, whether before or after irradiation, follow semiconductor behavior, where the conductivity increases exponentially with increasing temperature (18, 19).

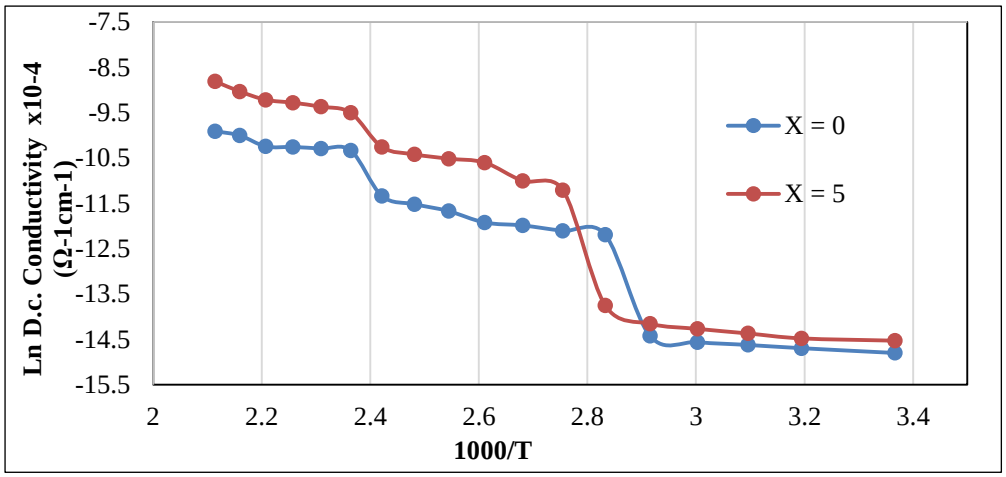

Figure 5. Electrical conductivity (DC) Ln (σ) of $Se_{70}Se_{30-x}Pb_x$ as a function of 1000/T with concentration ratio (X = 0 and 5) after irradiation

Tables 1 and **2**, **Figures 4** and **5** highlight the relationship between temperature and DC electrical conductivity Ln(σ) of $S_{70}Se_{30-X}Pb_X$ glass samples with concentrations (X = 0 and 5) before and after exposure to thermal neutron irradiation. The conductivity curves before and after irradiation in **Figures 4, 5** reveal three distinct conductivity regions related to low, medium, and high temperatures. These regions indicate the presence of multiple electrical conduction mechanisms (10, 11). Before and after irradiation, wherein the temperature range is between 297 K and 353 K, the conductivity increases gradually, and then a significant increase occurs between 353 K and 423 K. After 423 K and up to 473 K, the conductivity rises rapidly.

The change in conductivity curves at low temperatures (297-353 K) is because the charge carriers gain enough energy to transition between localized states near the Fermi level. This process takes place at a relatively low energy activation, gradually increasing conductivity (14, 20). However, above 353 K, the charge carriers become more mobile due to the higher

temperature and gain more energy, allowing conduction to occur via band-tail hopping. In the range of 353 K to 423 K, conduction is mainly driven by the variable-range-hopping (VRH) mechanism. At higher temperatures, between 423 K and 473 K, conduction is dominated by a thermally assisted process. This process involves the transition of electrons between extended states in the conduction and valence bands. The observed behavior is consistent with the theoretical predictions shown in **Equation 2** (15, 21).

$$\sigma = \sigma_{01} e^{(-\frac{E_1}{KT})} + \sigma_{02} e^{(-\frac{E_2}{KT})} + \sigma_{03} e^{(-\frac{E_3}{KT})} \quad (2)$$

The logarithmic relationship between electrical conductivity and absolute temperature is shown in **Figure 4** before irradiation and **Figure 5** after irradiation, showing how the electrical conductivity Ln (σ) and 1000/T change. The data show that all samples, whether before or after irradiation, follow the behavior of semiconductors, where the conductivity increases exponentially with increasing temperature according to **Equation 2** (18, 19).

Before irradiation, we note from **Figure 4** that the first sample with concentration (X = 0) has an increase in electrical conductivity with the increase in temperature from (297-353) K for the three regions shown in **Table 1** and **Figure 4**, which reinforces the fact that the compound is a semiconductor. As for after irradiation, we note from **Figure 5** and at concentration X = 0 that this sample behaves the same as before irradiation, such that its conductivity decreases with the increase in temperature from (297- 473) K for the three regions. However, when comparing the results for this sample after irradiation with the results before irradiation, we note that its conductivity has decreased, as we note from that that this sample has been affected by the radiation dose, so its electrical conductivity has decreased.

This can be explained. This change is due to the rearrangement of the atoms because of their collision with neutrons, which leads to the material gaining additional energy. This results in a decrease in conductivity. The data also indicates a nonlinear relationship between ln σ and 1000/T, which arises from multiple defects at grain boundaries due to imperfect atomic bonding. These defects lead to the trapping of charge carriers at low temperatures, while the density of states near the Fermi level improves the mobility of carriers at high temperatures by reducing the trapping and potential barriers (23, 24).

The slope of the curves was analyzed within three temperature ranges, namely low (297–353) K, medium (353–423) K, and high (423–473) K, to determine the activation energies (E_1, E_2, E_3) of the pre-factor (σ_{01}, σ_{02}, σ_{03}) of the S70Se30-XPbX glass alloy. As mentioned earlier, the curves indicate the existence of three separate paths, each characterized by a different slope associated with a specific activation energy. According to Equation (1), the slope of the graph of ln σ versus 1000/T can be used to determine the activation energies (E_1, E_2, E_3) according to the substitution ratio. Furthermore, the equation allows the calculation of the pre-factor (σ_{01}, σ_{02}, σ_{03}) within the three temperature ranges. These factors can be determined from the length of the curves and their points of intersection with the Y-axis, when the calculated values of these factors are shown in **Tables 1** and **2**.

Table 1. shows the data obtained from **Figure 4** after applying Equation 1 and calculating both the activation energies (E_1 , E_2, E_3) and the pre-exponential factor $\sigma_{01}, \sigma_{02} and\ \sigma_{03}$ that causes the partial substitution exponent before irradiation.

X	$E_{1\ ext}$ (eV)	$\sigma_{01\ ext}$	$E_{2\ Loc}$ (eV)	$\sigma_{02\ Loc}$	$E_{3\ Fermi}$ (eV)	$\sigma_{03\ Fermi}$
0	0.382411231	8.53048E-05	0.367287712	4.26524E-05	0.446345053	4.32706E-07
5	0.392668739	6.63482E-05	0.368315975	4.14676E-05	0.416615234	1.14833E-06

Table 2. shows the data of activation energies E_1, E_2, E_3 and the pre-exponential factor, σ_{02} *and* σ_{03} for $S_{70}Se_{30-X}Pb_X$ glass samples after irradiation.

X	**E1 $_{ext}$ (eV)**	$\boldsymbol{\sigma}$ **$_{1\ ext}$**	**E2$_{Loc}$ (eV)**	$\boldsymbol{\sigma}$**$_{2\ Loc}$**	**E3$_F$ (eV)**	$\boldsymbol{\sigma}$**$_{3\ Fermi}$**
0	0.4044106	4.97611E-05	0.3772637	3.24529E-05	0.371437819	5.06046E-06
5	0.3595702	1.40E-04	0.3468618	7.46417E-05	0.418872605	1.06631E-06

To calculate the energy state densities in three different regions - localized N (E_{loc}), extended N (E_{ext}), and Fermi level N (E_F). According to the ratio of substitution of the values of the constants (electron charge e, electron mass and values σ_{01}, σ_{02}, σ_{03}) in the equations in references (13, 14) mentioned below, the energy state densities in three different regions - local, extended, and Fermi level - were calculated. According to the following equations:

$$N(E_{ext}) = \left[\frac{6m}{e^2\hbar}\right] \sigma_{o\ ext.} \quad (3)$$

$$N(E_{loc}) = \left[\frac{6}{e^2 . f_{ph} . R^2}\right] \sigma_{0\ loc} \quad (4)$$

$$N(E_F) = \left[\frac{6}{e^2\ f_{ph}\ R^2}\right]\ \sigma_{o\ Fermi} \quad (5)$$

Where ($\hbar = 1.0545 \times 10^{-34}$ J.s) , f_{ph} is the phonon frequency, which is of order 10^{13} $s^{-1}$and R is the hopping distance and is , given by $R = 0.7736[\frac{\Delta E a^{-1}}{N(E_C)(KT)^2}]^{0.25}$ and $a^{-1} = 10$ A^0.

The three equations 3, 4, 5 were applied to calculate both the extended and localized state densities and at the Fermi level after substituting the constants in the equations before and after irradiation of the samples. The values calculated from these equations are recorded in **Tables 3** and **4.**

Table 3. shows the relationship between the density of extended states $N(E_{ext})$, $N(E_{fermi})$ and $N(E_{loc})$ upon partial substitution of selenium by lead before irradiation

x	**Tail Width ΔE**	**R**	**a**	**N(E_{ext})**	**N(E_{loc})**	**N(E_F)**
	(ev)	(A^0)	(A^0)	($ev^{-1}cm^{-3}$)	($ev^{-1}cm^{-3}$)	($ev^{-1}cm^{-3}$)
0	0.015123519	0.893410845	1.1854	4.40381E+21	1.25243E+21	1.12E+07
5	0.024352764	1.07167029	1.5241	3.42518E+21	8.46249E+20	2.25E+05

Table 4. The density of extended states $N(E_{ext})$, $N(E_{fermi})$ and $N(E_{loc})$ upon partial substitution of selenium by lead after irradiation

x	**Tail Width ΔE**	**R**	**a**	**N(E_{ext})**	**N(E_{loc})**	**N(E_F)**
	(ev)	(A^0)	(A^0)	($ev^{-1}cm^{-3}$)	($ev^{-1}cm^{-3}$)	($ev^{-1}cm^{-3}$)
0	0.027147441	1.183289564	2.032156581	2.56889E+21	5.43229E+20	6.00E+02
5	0.004564099	0.575727862	6.77385527	7.70666E+21	4.22229E+21	3.00E+05

It is noted from **Table 3** that when the lead concentration is equal to zero, the width of the energy tail before irradiation is equal to 0.0151 (eV), while at concentration 5, the width of the energy tail increases to 0.024352764 (eV). This means that the partial replacement of selenium with lead affects the crystalline structure of the alloys and thus leads to a change in the physical properties. This is consistent with the results for the jump distance R, as the value of R at concentration zero is equal to 0.893410845 A^0, while at concentration 5, the jump distance R is equal to 1.07167029 A^0. From **Table 4**, after irradiation and when the lead concentration is zero, the width of the energy tail is 0.02714744 A^0 electron volts, while when the concentration increases to 5, the width of the energy tail decreases to 0.004564099 (eV). This means that irradiation rearranges the atoms in the alloy because the ion bombardment has radiation energy that is converted into heat, affecting the alloy's crystalline structure (25). As for the jump distance R, we notice that its value at zero concentration after irradiation is equal to 1.183289564 A^0, while at concentration 5, the jump distance R after

irradiation is equal to 0.575727862 A^0.

Table 3 discusses the results of the density of states before irradiation. We note that at zero concentration, the density of extended states N (E_{ext}) is equal to 4.40381E+21 (eV^{-1} cm^{-3}). When the concentration increases to 5, it decreases and becomes ($ev^{-1}cm^{-3}$) 3.42518E+21. Also, from the same table before irradiation at zero concentration, the density of local states N(E_{loc}) is equal to 1.25243E+21 ($eV^{-1}cm^{-3}$). When the concentration is 5, it increases and becomes 8.46249E+20 ($eV^{-1}cm^{-3}$). Also, from the same table before irradiation at zero concentration, the density of local states N(E_{loc}) is equal to 1.25243E+21 ($eV^{-1}cm^{-3}$). When the concentration is 5, it increases and becomes 8.46249E+20 ($eV^{-1}cm^{-3}$). Also, from the same table before irradiation, we note that at zero concentration, the density of states at the Fermi level N(E_{fermi}) is equal to 1.12E+07 ($eV^{-1}cm^{-3}$). When the concentration increases to 5, it decreases and becomes 2. 25E+05 ($ev^{-1}cm^{-3}$).

Now, from **Table 4**, we discuss the results of the density of states after irradiation. At zero concentration, the density of extended states N(E_{ext}) is equal to 2.56889E+20 ($eV^{-1}cm^{-3}$). At 5 concentrations, it increases and becomes 7.70666E+21($ev^{-1}cm^{-3}$). Also, from the same table, after irradiation and at zero concentration, the density of local states N(E_{loc}) becomes 5.43229E+20 ($eV^{-1}cm^{-3}$). When the concentration increases to 5, the density of local states N(E_{loc}) equals 4.22229E+21 ($eV^{-1}cm^{-3}$), and from the same table, after irradiation and at zero concentration, the density of states at the Fermi level N(E_{fermi}) equals 6.00E+02 ($eV^{-1}cm^{-3}$). As for the concentration 5 after irradiation, it increases and becomes 3.00E+05 ($eV^{-1}cm^{-3}$).

By analyzing the previous results for the density of extended and localized states at the Fermi level and according to the concentration ratio (X = 0 and 5), we notice that there is a variation and difference in the density of states and this is attributed to several factors, such as changing the energy gap, or the width of the tails, or the concentration of the conductive material, or a change in the properties of the conductor. It was found from these results that the best density of states before irradiation is for the extended states when the lead concentration (X = 0) is because the energy gap is small at the extended levels at this concentration, to takes the preferred value. It was also noted that the energy levels of all extended and localized states and at the Fermi level change with the change in concentration, as these levels depend on the strength of the bond between the atoms. The more the bonds are equivalent and interconnected with each other, the less randomness in the crystal structure, and the higher the crystallization rate in the alloys. When the lead ratio changes, this leads to a change in the width of the tails of the bundles, and this change in the width of the tails of the bundles leads to pulling them outside the energy gap, so they become extended states. As for the increase in the tails of the bundles, this leads to the extension of these tails within the energy gap, as indicated by researchers (4, 5). From this, we conclude that the process of partial replacement of selenium with the lead element led to the ability to control the reduction or increase in randomness according to the ability of the bonds that lead is linked to. If the bonding process is high, the randomness decreases, and crystallization increases. On the contrary, if the dangling bonds in the alloy increase, then the randomness will increase, leading to increased disorder and thus increased density of local states at the Fermi level. This is because the valence bands in chalcogenide glasses contain a high proportion of (unshared) electronic states called lone pairs and the process of substitution or introduction of other elements in chalcogenide alloys where the valence electrons near the more electronegative atoms have higher energies than those near the atoms with a high electrical charge, it has been observed that partial substitution affects the width or narrowing of the tail of the bands and the width may be similar to the valence bands and the tail of the bands

changes as a result of the increase or decrease in the types of bonds in the alloys and this may lead to an increase or decrease in the edge of the conduction or valence band, which affects the local and extended state densities. The increase in the density of localized states and the decrease in the extended states at the Fermi level greatly affect the crystal structure of the lattice, transforming it from the amorphous state to the polycrystalline state, which reduces the randomness of the crystal structure in samples irradiated with thermal neutrons (16).

To discuss the previous results after irradiation, we note that there is a clear effect due to the effect of slow (thermal) neutron radiation on the density of states of the Se70Se30-xPbx alloy, depending on the concentration of zero and 5, for both extended and localized states, as well as at the Fermi level. We note that the density of extended states after irradiation decreased at the concentration of zero while it increased at the concentration of 5, while the density of localized states after irradiation decreased at the concentration of zero while it increased at the concentration of 5, while the density of states at the Fermi level after irradiation, the density of states at the concentration of zero decreased while it increased at the concentration of 5, and this is mainly due to the modification of the atomic structure, as slow neutrons carry relatively low energy, which allows them to interact selectively with the nuclei in the material without destroying the structure. These interactions may lead to the displacement of atoms from their original positions within the lattice (25), causing a rearrangement of chemical bonds. In amorphous materials (such as chalcogenides), this leads to changes in the local structure of the bonds, which are reflected in the density of electronic states. (26) This change and variation in the density of the three states can be enhanced by an increase or decrease in the density of states at the energy band edge. The density of states near the conduction band or valence band edge can be directly affected by the redistribution of bonds (27). Radiation can lead to an increase in the number of unsaturated bond states (28), reducing the long-range order, causing changes in the energy gap (29). Neutron radiation creates new states within the energy gap, which act as “metastatic energy levels,” changing the electrical conductivity of the material. (30) These effects depend on the radiation dose. Some properties may be improved by gap filling or redistribution of impurities (31).

4. Conclusion

This article discusses the effect of partial substitution and thermal neutron irradiation on the density of local and extended states and the Fermi level in $S_{70}Se_{30-x}Pb_x$ alloy with x ratios (0, 5) prepared by the melting point method. By analyzing the electrical conductivity over different temperature ranges, three distinct conduction mechanisms were identified, related to the local $N(E_{ext})$ and $N(E_{loc})$ extended states and the Fermi level $N(E_F)$ at high, medium, and low temperatures. The results showed that all of these state densities are significantly affected by the substitution ratio and significantly by the thermal neutron radiation dose due to the movement of carriers between the extended states in the conduction and valence bands as well as due to the change in the width of the energy tails and the hopping distance of the electrons as well as the activation energy. The electrical conductivity constants, the energy band gap, the tail width EΔ, the hopping distance R and the interatomic distance a were calculated. All of them were found to change with the change in the lead concentrations and the thermal neutron radiation dose.

Acknowledgment

We extend my thanks to the College of Education for Pure Sciences, Ibn Al-Haitham, and the University of Baghdad for assisting in completing this work by opening private laboratories and providing scientific facilities by the staff of the Physics Department to help support the research project.

Conflict of Interest

The authors declare that they have no conflicts of interest.

Funding

None.

References

1. Tohge N, Matsuo H, Minami T. Electrical properties of n-type semiconducting chalcogenide glasses in the system Pb-Ge-Se. J Non-Cryst Solids. 1987;95:809–16. https://doi.org/10.1016/S0022-3093(87)80685-3.
2. Tohge N, Kanda K, Minami T. Formation of chalcogenide glass p-n junctions. Appl Phys Lett. 1986;48(25):1739–41. https://doi.org/10.1063/1.96820.
3. Street RA, Mott NF. States in the gap in glassy semiconductors. Phys Rev Lett. 1975;35(19):1293. https://doi.org/10.1103/PhysRevLett.35.1293.
4. Mott NF, Davis EA. Electronic processes in non-crystalline materials. Oxford: OUP Oxford; 2012.
5. Mott NF. Introductory talk; Conduction in non-crystalline materials. J Non-Cryst Solids. 1972;8:1–8. https://doi.org/10.1016/0022-3093(90)90112-3.
6. Vikhrov S, Nagels P, Bhat PK. n-Type conduction in chalcogenide glasses of the Ge-Se-Bi system. In: Recent Developments in Condensed Matter Physics. Vol. 2. Boston (MA): Springer; 1981. p. 333–40. https://doi.org/10.1007/978-1-4684-3899-4_42.
7. Tohge N, Minami T, Tanaka M. Photoconductivity of vitreous chalcogenides chemically modified by bismuth. J Non-Cryst Solids. 1983;59:999–1002. https://doi.org/10.1016/0022-3093(90)90335-6.
8. Mohammed JS. Investigating the optical and electrical characteristics of As60Cu40-xSex thin films prepared using pulsed laser deposition method. Chalcogen Lett. 2023;20(7):449–58. https://doi.org/10.15251/CL.2023.207.449.
9. Jasim KA, Makki SA, Abud Almohsin A. Comparison study of transition temperature between the superconducting compounds Tl0.9Pb0.1Ba2Ca2Cu3O9-δ, Tl0.9Sb0.1Ba2Ca2Cu3O9-δ and Tl0.9Cr0.1Ba2Ca2Cu3O9-δ. Phys Procedia. 2014;55:336–41. https://doi.org/10.1016/j.phpro.2014.07.049.
10. Ahmed BA, Mohammed JS, Fadhil RN, Jasim KA, Shaban AH, Al Dulaimi AH. The dependence of the energy density states on the substitution of chemical elements in the Se6Te4-xSbx thin film. Chalcogen Lett. 2022;19(4):301–8. https://doi.org/10.15251/CL.2022.194.301.
11. Khudhair NH, Jasim KA. Study the effect of tin on the energy density of states of Se60Te40-xSnx chalcogenide glass. AIP Conf Proc. 2023;2769(1). https://doi.org/10.1063/5.01129373.
12. Khudhair NH, Jasim KA. Preparation and study the effect of Sb on the energy density of states of Se60Te40. AIP Conf Proc. 2023;2769(1). https://doi.org/10.1063/5.0129550.
13. Wadi KM, Hasan MA, Aneed SH, Faraj MG, Jasim KA. Synthesis and Analysis of the Density States and Optical Characteristics of Se100-X TeX Semiconductors. ARO-THE SCIENTIFIC JOURNAL OF KOYA UNIVERSITY. 2025 May 5;13(1):175-84.
14. Ahmed BA, Mohammed JS, Fadhil RN, Jasim KA, Shaban AH, Al Dulaimi AH. The dependence of the energy density states on the substitution of chemical elements in the Se6Te4-xSbx thin film. chalcogenide Letters. 2022 Apr 1;19(4):301-8.
15. Chillab RK, Jahil SS, Wadi KM, Jasim KA, Shaban AH. Fabrication of Ge30Te70-xSbx glass

alloys and studying the effect of partial substitution on DC electrical energy parameters. Key Eng Mater. 2021;900:163–71.
16. Abdulmajeed MA, Azzawi JH, Jasim KA. Study the physical properties of Se65Sn35-xTex alloys. InAIP Conference Proceedings 2025 Aug 20 (Vol. 3321, No. 1, p. 020010). AIP Publishing LLC.
17. Mohammed MA, Aklo KN, Watan AW, Jasim KA, Salman EM. Effect of Thermal Neutron Radiation Dose on Density of Local and Extended Energy States in Se55S20Sb15Sn10 Alloy. Iraqi Journal of Applied Physics. 2024 May 20;20(2B):393-8.
18. Adler D. Disordered materials: amorphous and liquid semiconductors. In: Tauc J, editor. Plenum, New York: Science. 1975;188(4184):141–2. https://doi.org/10.1126/science.188.4184.141.
19. Lee JK, Park SD, Kim BS, Oh MW, Cho SH, Min BK, Lee HW, Kim MH. Control of thermoelectric properties through the addition of Ag in the Bi0.5Sb1.5Te3 alloy. Electron Mater Lett. 2010;6:201–7. https://doi.org/10.3365/2010.12.201.
20. Mobarak M, Shaban HT, Elhady AF. Electrical and thermoelectric properties of CuInS2 single crystals. Mater Chem Phys. 2008;109(2–3):287–90. https://doi.org/10.1016/j.matchemphys.2007.11.025.
21. Kadhim BB, Risan RH, Shaban AH, Jasim KA. Electrical characteristics of nickel/epoxy-Unsaturated polyester blend nanocomposites. Technologies and Materials for Renewable Energy, Environment and Sustainability: TMREES19. 2019.
22. Paul DK, Mitra SS. Evaluation of Mott's parameters for hopping conduction in amorphous Ge, Si, and Se–Si. Phys Rev Lett. 1973;31(16):1000. https://doi.org/10.1103/PhysRevLett.31.1000.
23. Jassim KA, Jassim WH, Mahdi SH. The effect of sunlight on medium density polyethylene water pipes. Energy Procedia. 2017;119:650–5. https://doi.org/10.1016/j.egypro.2017.07.091.
24. Mott NF, Davis EA. Electronic processes in non-crystalline materials. Oxford: OUP Oxford; 2012.
25. Ali MH, Mohammed FG, Al-Saady YI. Water reservoir techniques using remote sensing and GIS: a literature survey. J Physics: Conf Series 2024; 2857: 012022.
26. Al-Ewaisi MA, Imran MM, Lafi OA, Moh'd WK. Effect of gamma irradiation on some electrical properties and optical band gap of bulk Se92Sn8 chalcogenide glass. Phys B Condens Matter. 2010;405(12):2643–7. https://doi.org/10.1016/j.physb.2010.03.045.
27. Jasim KA, Shaban AH. The Effect of Gamma Radiation on the Manufactured. Materials for Sustainability. 2022:41.
28. Vali IP, Shetty PK, Mahesha MG, Rao MN, Kesari S. Thermal neutron irradiation effects on structural and electrical properties of n-type 4H–SiC. J Mater Sci Mater Electron. 2020;31:8496–501. https://doi.org/10.1007/s10854-020-03385-9.
29. Al Refaei DH, Najam LA, Al Taan LM. The effect of neutron irradiation on optical, structural and morphological properties of cadmium selenide thin films. J Rad Nucl Appl. 2021;6:207–16. https://www.naturalspublishing.com/files/published/322x14391h4pyn.pdf.
30. Salim FM, Ghadhban RQ, Aklo KN, Jasim KA. Physical properties of HgX Sb1-X Ba2Ca2Cu3O8+ δ superconducting compound: Effect of fast neutrons irradiation. AIP Conf Proceedings 2019; 2123(1): 020080. AIP Publishing LLC.
31. Noori RI, Mahdi HA, Abdullah MD, Jasim KA. Analyze the Structure and Electrical Properties of $PbBr_2$ Ca1. 9Sb0. 1Cu3O8+ δ Superconducting Gamma Irradiation. J Physics: Conf Series 2024; 2754(1): 012014. IOP Publishing.